A Logical Molecular Circuit for Programmable and Autonomous Regulation of Protein Activity Using DNA Aptamer−Protein Interactions

Da Han,[‡,§] Zhi Zhu,[†,⊥,§] Cuichen Wu,[‡] Lu Peng,[‡] Leiji Zhou,[‡] Basri Gulbakan,[‡] Guizhi Zhu,[†,‡] Kathryn R. Williams,[‡] and Weihong Tan*[,‡,†]

[†]Molecular Science and Biomedicine Laboratory, State Key Laboratory of Chemo/Biosensing and Chemometrics, College of Biology and College of Chemistry and Chemical Engineering, Hunan University, Changsha 410082, China

[‡]Department of Chemistry and Department of Physiology and Functional Genomics, Center for Research at the Bio/Nano Interface, Shands Cancer Center and UF Genetics Institute, University of Florida, Gainesville, Florida, 32611-7200, United States

[⊥]Department of Chemical Biology, College of Chemistry and Chemical Engineering, Xiamen University, Xiamen 361005, China

Ⓢ Supporting Information

ABSTRACT: Researchers increasingly envision an important role for artificial biochemical circuits in biological engineering, much like electrical circuits in electrical engineering. Similar to electrical circuits, which control electromechanical devices, biochemical circuits could be utilized as a type of servomechanism to control nanodevices in vitro, monitor chemical reactions in situ, or regulate gene expressions in vivo.[1] As a consequence of their relative robustness and potential applicability for controlling a wide range of in vitro chemistries, synthetic cell-free biochemical circuits promise to be useful in manipulating the functions of biological molecules. Here, we describe the first logical circuit based on DNA−protein interactions with accurate threshold control, enabling autonomous, self-sustained and programmable manipulation of protein activity in vitro. Similar circuits made previously were based primarily on DNA hybridization and strand displacement reactions. This new design uses the diverse nucleic acid interactions with proteins. The circuit can precisely sense the local enzymatic environment, such as the concentration of thrombin, and when it is excessively high, a coagulation inhibitor is automatically released by a concentration-adjusted circuit module. To demonstrate the programmable and autonomous modulation, a molecular circuit with different threshold concentrations of thrombin was tested as a proof of principle. In the future, owing to tunable regulation, design modularity and target specificity, this prototype could lead to the development of novel DNA biochemical circuits to control the delivery of aptamer-based drugs in smart and personalized medicine, providing a more efficient and safer therapeutic strategy.
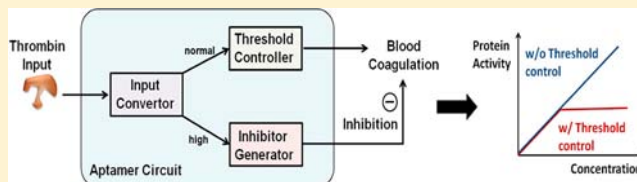
INTRODUCTION

Nucleic acids, as carriers of genetic information with well-regulated and predictable structures, are promising materials for the design and engineering of biochemical circuits. In particular, by emulating the digital logic found in typical circuit boards, recent reports demonstrated that DNA-based biocircuitry could perform logic gate operations, signal restoration, amplification, feedback, and cascading, all by distinct DNA strands.[2−6] Recently, their ability to interact with naturally occurring biomolecules, together with such unique properties as programmability, Boolean processing capability, nanometric size, and autonomous operation, has opened a novel and exciting direction in biological and biomedical applications.[7−12] Various circuits with single-purpose or generic computing capability have been demonstrated using nucleic acid (NA) base pairing interactions. Examples include RNA-based logic devices for processing cellular information[13] and quantitatively programming gene expression,[14] as well as a DNA-based biocomputer for logical analysis of multiple mRNA to trigger corresponding cellular response.[15] Such devices demonstrated

the programmability and versatility of NA circuits for further development toward the goal of logically analyzing a complex biological environment and precisely regulating the actuation of cellular behaviors. While these NA-based circuits are of great scientific interest, they are primarily based on nucleic acid hybridizations and strand displacement reactions between NA probes of different lengths. This has severely restricted circuit operation solely to genetic molecules.

Inspired by these advances, but distinct from their operation at the level of gene expression by DNA hybridization, we sought to explore the interactions between NA and other molecules such as proteins in cell-free logical circuit operation. There are two significant issues of interest: the first is to understand whether NA−protein interactions can be programmably enrolled in molecular circuits; and the second is to apply the capability of the logic circuit to directly perform precise and smart manipulation of the functions of proteins, which are often
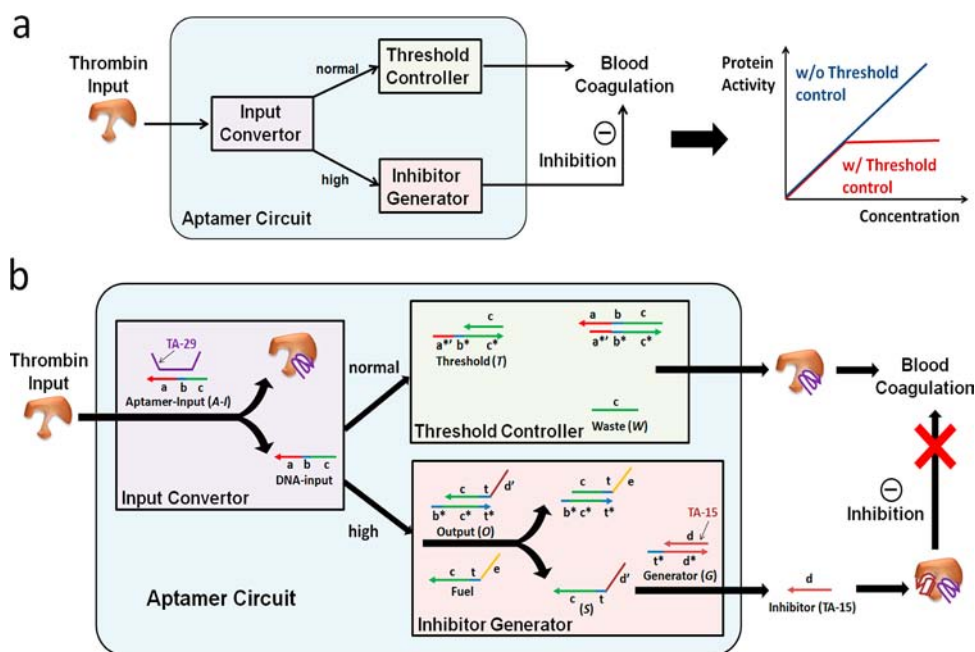
Figure 1. Working Scheme of molecular circuit. (a) Diagram illustrating circuitry. The circuit consists of three modules, **Input Convertor**, **Threshold Controller** and **Inhibitor Generator**, which can be programmed with threshold control for smart manipulation of protein activity. (b) Working scheme for molecular circuit, driven by a series of DNA displacement reactions. Colored lines indicate DNA strands with different domains. TA-29 and TA-15 are two thrombin aptamers with different functions, including recognition and inhibition, respectively. All **x** domains are complementary to **x***; **b*** and **t*** are short toehold domains with 5-nt; **a*′b*** is a long toehold domain with 10-nt; **c*** and **d*** are recognition domains with 15-nt. *A-I*, *T*, *O* and *G* are initially present as duplex components, along with ssDNA *Fuel*.

more important than genetic molecules because proteins are at the centers of homeostatic systems and the key regulators of an organism's behaviors.

A major challenge for direct protein manipulation by NA logic circuitry is to find a key component that can bridge nucleic acids with proteins without influencing the programmability and versatility of logic circuits. A common regulation paradigm used in previous reports is genetic regulation of protein expression, which requires sophisticated and cell-wide coordination.[16−18] However, a special single-stranded oligonucleotide, commonly known as an aptamer, has the potential to interact with proteins specifically and is thus explored and developed in this report to build a simple and effective molecular circuit for manipulation of protein functions and activities. Aptamers, obtained via an in vitro selection strategy called systematic evolution of ligands by exponential enrichment (SELEX), can extend the recognition capabilities of nucleic acids from Watson−Crick base-pairing to interactions with various targets, such as small molecules, proteins, and even viruses or cells, via the aptamer's unique secondary or tertiary structure.[19−21] In addition, the affinity and specificity of an aptamer can be tuned through the selection process or by postselection sequence optimization in order to meet the specific performance requirements of a given application. Finally, some aptamers are not only able to recognize the target proteins but can also regulate protein functions.[22−24] Such aptamers are regarded as potential drugs with protein regulation functions or drug carriers for many diseases and are already in the pipeline for clinical use, including PDGF and VEGF aptamers for controlling the age-related macular degeneration,[25,26] demonstrating their reliability for biomedical applications. Since an aptamer is essentially a single-stranded oligonucleotide, it is convenient for logic circuit design, just as previous NA-based circuits. Aptamers can be directly used as

building blocks to fabricate seamless logic-based aptamer circuits with enhanced capabilities and an extended scope of applications, from simple NA base-pairing reactions to more complicated biomolecular reactions such as NA-protein or NA-small molecule interactions.

As a proof of concept, human α-thrombin, which initiates blood coagulation process by converting fibrinogen to fibrin, was chosen as our model target protein. Imbalances in thrombin levels can lead to a variety of functional disorders, and even death. For example, thrombin excesses can result in life-threatening blood clots in key organs.[27] Consequently, the design of safe and effective anticoagulants would have a significant effect on clinical therapy. However, dosage control, where imprecision can lead to severe side effects, is a challenge for traditional anticoagulants. Therefore, inspired by the negative feedback loop concept of biological signaling pathways, in which a signal bias induces the expression of its own inhibitor, we designed a logic-based molecular circuit that can precisely sense the local enzymatic environment (i.e., the concentration of thrombin in the present example) and smartly control its coagulation function by a concentration-triggered threshold control module, which has the potential to provide a more efficient and safer therapeutic strategy.

The operating principle of our molecular circuit for protein regulation is schematically illustrated in Figure 1a. In general, a programmable and autonomous circuit with threshold control was constructed of three DNA modules: an **Input Convertor** that converts the protein input to DNA input for downstream cascade reactions; a **Threshold Controller** that sets the threshold concentration for the system to maintain regular protein activity; and an **Inhibitor Generator** that inhibits excessively high protein activity once it surpasses the threshold. This circuit can intelligently sense the environment, i.e., the concentration of protein, and initiate the inhibitory function
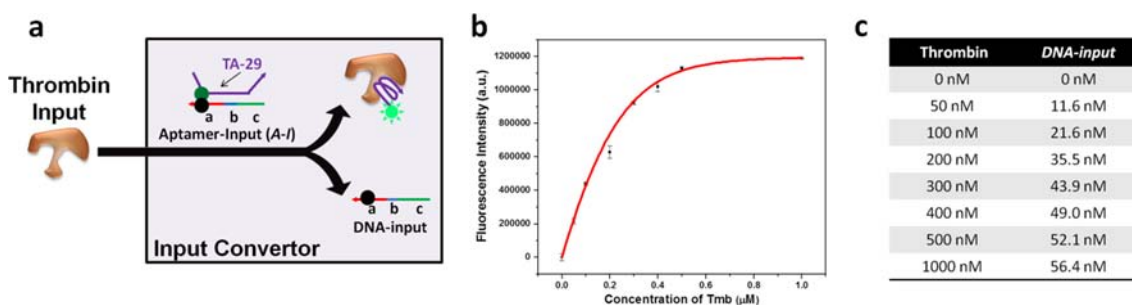
Figure 2. (a) Scheme of FRET-based thrombin sensor in the **Input Convertor** module. Quencher-labeled *DNA-input* and fluorophore-labeled TA-29 can be dehybridized by thrombin. (b) Plot of the fluorescence restoration of 100 nM *A-I* with different concentrations of thrombin. (c) Relationship between different concentrations of thrombin and released *DNA-input*. The concentration of *A-I* is 100 nM.

through a threshold control loop when excessively high protein concentration occurs. By setting the threshold value according to each practical situation, the circuit may be usable as a smart drug delivery system in the design of personalized medicine.

To demonstrate such intelligent regulatory function with thrombin as a model, two anti-thrombin aptamers are employed to build an aptamer circuit to smartly control coagulation: a 29mer (TA-29) that binds to the heparin exosite without inhibitory function and a 15mer (TA-15) that binds to the fibrinogen exosite with strong inhibitory function.[28,29] In the detailed design (Figure 1b), the circuit includes a series of aptamer and DNA displacement reactions, in which a single-stranded DNA (ssDNA) can be displaced from the initial duplex by an even stronger binder, either a protein molecule or a better matched DNA strand.[5,30,31] The circuit starts with the introduction of thrombin. In the **Input Convertor**, thrombin reacts with duplex *Aptamer-Input* (*A-I*), which contains TA-29 partially hybridized with a piece of ssDNA. This ssDNA, termed as *DNA-input*, is released from *A-I* by competitive binding of thrombin to TA-29, converting the protein input to DNA input for the following cascade reactions.

The *DNA-input* then enters the **Threshold Controller** module and rapidly reacts with duplex *Threshold* (*T*) via an exposed toehold a*′b* to generate inert ssDNA *Waste* (*W*) without further reaction. Through this bypass route, thrombin only binds with TA-29 and thus can still perform its normal catalytic function in blood coagulation. However, after *T* is depleted, the excess *DNA-input* will continue to the **Inhibitor Generator** module, in which *DNA-Input* reacts with duplex *Output* (*O*) via exposed toehold b*, thereby triggering the amplification reaction of *O* with *Fuel* (*F*), which helps to catalytically produce the output (Figure S1, Supporting Information). The released product, which is denoted as *S* (ctd′) with effective toehold t, then cascades to duplex *Generator* (*G*), followed by the release of the *Inhibitor* TA-15 to inhibit thrombin coagulation.

The sequential order of these reactions is precisely controlled by the differences in thermodynamic stability, as well as reaction kinetics, between each component. In this system, stability is mainly determined by the length of exposed toehold. For instance, both *T* and *O* can react with *DNA-input*, but the reaction of *DNA-input* with *T* is more favorable than its reaction with *O*, based on the longer toehold of *T* (a*′b*) compared to *O* (b*). As a result, more thermodynamically stable duplex strands will be formed between the *DNA-input* and *T* (a*′b*c). The difference in thermodynamic stability is also reflected in the reaction kinetics. In this case, the 10-nucleotide (10-nt) toehold in *T* provides a displacement

reaction rate about 100 times higher than that of the 5-nt toehold in *O*.[30] As a result, the **Inhibitor Generator** can only work when the **Threshold Controller** is completely consumed.

An additional concern is the need for sufficient concentration of *O* to produce an adequate response. To ensure this reaction, an entropy-driven amplification strategy is introduced via the *Fuel* strand in the **Inhibitor Generator**. *DNA-input* can transform free *Fuel* into output without being consumed, according to the reactions shown in the Figure S1.[5] Thus, a small amount of *DNA-input* can trigger the release of a large amount of inhibitor (TA-15). Furthermore, to avoid undesired leaking reactions, the lengths of certain strands were shortened (e.g., *d′* is shorter than *d*). Overall, by precisely and smartly programming the major duplex elements *A-I*, *T*, *O*, and *G* in the three modules, the aptamer circuit can work through an autonomous threshold control loop to generate *Inhibitor* TA-15 and intelligently regulate the activity of thrombin according to the preset threshold concentration.

RESULTS AND DISCUSSION

Validation of the Signal Transduction in Each Module. To ensure proper operation of the entire circuit, the signal transduction in each module was validated separately. The function of the **Input Convertor** is to transform the protein signal to a DNA signal for compatibility. Unlike DNA hybridization, the quantitative binding relationship between protein and aptamer depends on the K_d of the aptamer and cannot be simply regarded as a 1:1 ratio. Thus, a quantitative relationship needs to be established in order to set an appropriate threshold value for subsequent reactions. Motivated by the design of FRET-based aptamer biosensors,[32,33] a fluorophore (FAM) in the TA-29 strand and a quencher (DABCYL) in the *DNA-input* strand were coupled to quantify the released *DNA-input* triggered by thrombin (Figure 2a). The fluorescence enhancement generated by the dehybridization of duplex *A-I* was measured after addition of different concentrations of thrombin (Figure 2b). The resulting calibration curve (Figure S4) established the quantitative relationship between thrombin and released *DNA-input*, as shown in Figure 2c. This allowed the quantity of *DNA-input* generated from thrombin for subsequent reactions to be determined precisely.

Next, the performance of the **Inhibitor Generator** was verified by labeling *G* duplex with a fluorophore and quencher FRET-pair. As a result, when TA-15 is released from *G*, the fluorescence intensity of the system is restored. For this modular test, *DNA-input* was directly applied as input to activate the **Inhibitor Generator**. Before testing, all duplex
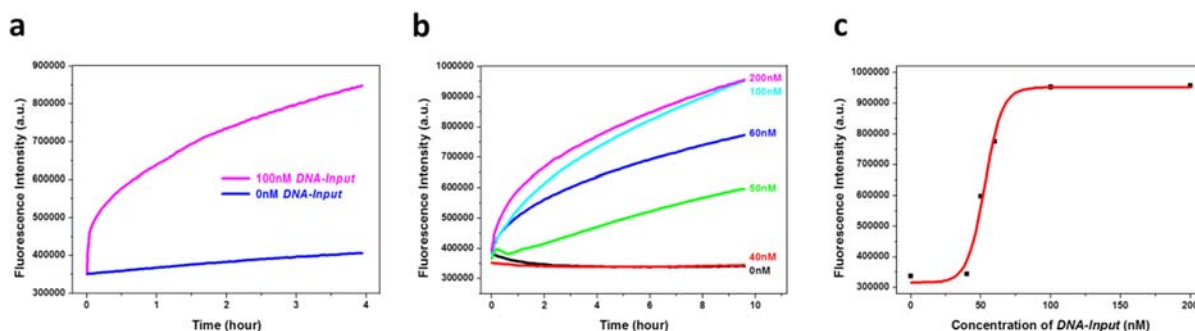
Figure 3. (a) Fluorescence kinetics studies of the signal transduction process in the **Inhibitor Generator** module. *O*, *G*, and *F* were mixed with concentrations of 100, 150, and 200 nM, respectively. Then 0 and 100 nM *DNA-input* were added to the mixture, and the fluorescence signal was monitored at 25 °C. (b) Fluorescence kinetics study of the signal transduction of the **Threshold Controller** together with the **Inhibitor Generator**. *T*, *O*, *G*, and *F* were mixed with concentrations of 40, 100, 150, and 200 nM, respectively. ssDNA *DNA-input* was added at different concentrations (0, 40, 50, 60, 100, and 200 nM), and the fluorescence was monitored with λ_{ex} (488 nm) and λ_{em} (518 nm). (c) Plot of output final fluorescence intensity versus concentration of *DNA-input*.

components were purified using gel electrophoresis to remove excess strands in order to avoid undesired system leakage. Then, *O* (100 nM), *G* (150 nM), and *F* (200 nM) were mixed in the buffer, and the fluorescence was monitored in the absence and presence of 100 nM *DNA-input*, as shown in Figure 3a. Without *DNA-input*, the **Inhibitor Generator** is stable for hours. Upon the introduction of *DNA-input*, an obvious fluorescence enhancement can be observed, indicating that the **Inhibitor Generator** module functions correctly and effectively. In addition, different concentrations of *DNA-input* were tested, showing a nonlinear fluorescence restoration with elevated concentration of *DNA-input* (Figure S5). The results demonstrate that the DNA cascade reactions can be driven forward with the catalytic effect of *Fuel*, thus generating a large amount of TA-15 with a low concentration of *DNA-input*.

By integrating the **Threshold Controller** with the **Inhibitor Generator**, a sequential reaction order with a sharp threshold value was expected. A threshold concentration of 40 nM was set in the **Threshold Controller** by adding 40 nM purified *T* duplex. The FRET-based *G* in the **Inhibitor Generator** was still applied as a reporter to visualize the signal readout. A series of different concentrations of *DNA-input* were introduced to verify the efficacy of threshold suppression in the presence of both modules. The fluorescence kinetics experiments (Figure 3b) exhibited fluorescence restoration starting from *DNA-input* concentration of 50 nM, and the input-versus-fluorescence plot (Figure 3c) clearly revealed a sharp threshold value at 40 nM, demonstrating the successful construction of a molecular circuit with precise threshold control.

Performance of the Entire Circuit with Thrombin as Input. After confirming the proper function of each component, we further tested the performance of the entire circuit with thrombin as input by fluorescence readout from the FRET-based *G*. According to the previous *DNA-input* quantitative results (Figure 2c), the concentration of *T* was set at either 20 or 35 nM, corresponding to the concentrations of *DNA-input* generated by 100 and 200 nM thrombin, respectively. When the concentration of thrombin is below the threshold value, only the **Threshold Controller** is functioning with no fluorescence enhancement. However, once the thrombin concentration exceeds the threshold value, depletion of the **Threshold Controller** and activation of the **Inhibitor Generator** occur, thus increasing the fluorescence intensity. In Figure 4, the fluorescence restoration started at thrombin
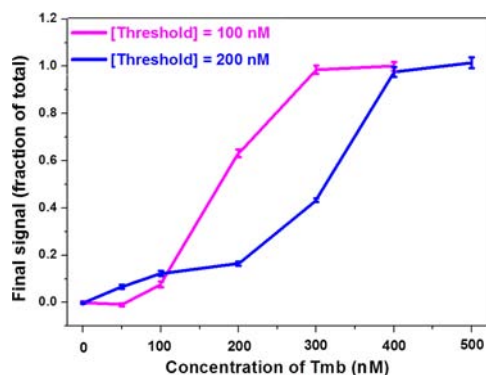
Figure 4. Fluorescence output versus thrombin concentration plot with two preset threshold values (concentration of Tmb) at 100 and 200 nM. Purified *A-I*, *O*, *G*, and *F* were mixed at the concentrations of 100, 100, 150, and 200 nM, respectively. Fluorescence signals were recorded with λ_{ex} (488 nm) and λ_{em} (518 nm) at 25 °C. The final fluorescence was normalized to the maximum completion level.

concentrations of 100 and 200 nM for the circuit with two different threshold concentrations, respectively, confirming that the circuit can function as designed and release TA-15 only when the thrombin concentration exceeds the predetermined threshold value.

Programmable and Autonomous Protein Regulation by Molecular Circuit. The concentrations of free thrombin observed *in situ* range from less than 1 nM to greater than 100–500 nM.[34,35] The local concentration of thrombin can even exceed 500 nM with the inducement of some thrombin-generating drugs. These high levels of thrombin cannot be removed from the body in a short time, thus leading to severe blood clotting. Therefore, a predetermined threshold value, above which the thrombin inhibition drug works, can effectively avoid excessively high thrombin activity, while, at the same time, maintaining regular coagulation function. To demonstrate that our circuit can realize such manipulation of thrombin function, a commercially available chromogenic peptide, β-Ala-Gly-Arg-p-nitroanilide diacetate, was chosen as the thrombin substrate. The catalytic activity of thrombin can be determined from the hydrolysis rate of the substrate by monitoring the absorbance of hydrolysis product p-nitroanilide at 405 nm.[36–38] The absorbance change (δA) after 30 min was recorded as the evaluation index of thrombin catalytic activity. The influence of the two aptamers, TA-15 and TA-29, on the catalytic function
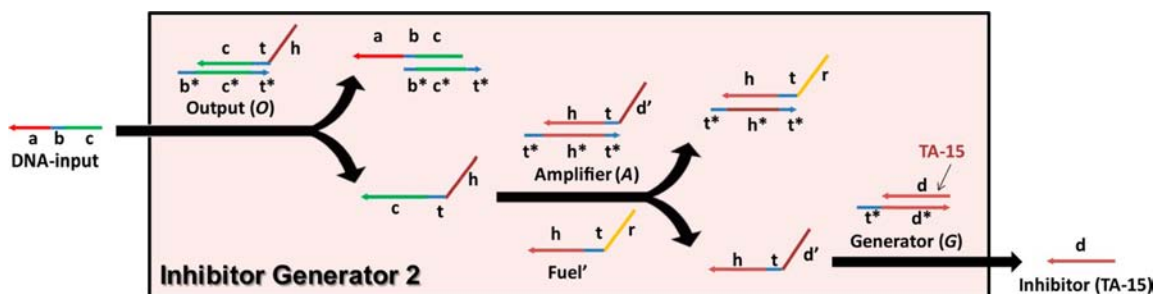
Figure 5. Working scheme of **Inhibitor Generator 2**. Duplex *A* and the *Fuel′* strand were designed to delay the amplification process for one step.

of thrombin was first investigated. The results (Figures S8 and S9) confirmed that TA-15 can inhibit the coagulation function of thrombin, while TA-29 has no inhibitory effect on thrombin.

As a result of sub-μM binding affinity of TA-15 to thrombin (Figure S9), at least 2-fold excess TA-15 is required to obtain more than 50% inhibition effect. In order to generate sufficient signal molecules for downstream reactions, the concentration of *O* may need to be elevated. However, in this scenario, *O* would be present at much higher concentration than *T*, possibly leading to failure of the **Threshold Controller** caused by the increased displacement reaction rate in the **Inhibition Generator**. Our initial attempt adapting the strategy of Figure 1 exhibited continuous inhibitory effect on thrombin catalytic activity without any threshold control (Figure S11). To solve this problem, a modified **Inhibition Generator** module was designed. Because of the modularity of the aptamer circuit, this modified **Inhibition Generator** module could simply replace the previous **Inhibition Generator** module without affecting the other two functional modules.

As shown in Figure 5, a duplex component, termed *Amplifier* (*A*) with its own catalytic strand *Fuel′*, was engineered and incorporated into the module to delay the amplification process for one step. In this case, *O* can be kept at its regular concentration to generate ssDNA **cth** in the presence of *DNA-input*. Then, the ssDNA **cth** displaces *A* with the help of *Fuel′* though an entropy-driven amplification cycle and releases a large amount of **htd′** strand, thus generating sufficient TA-15 for subsequent inhibition. Since *A* has no sequence similarity with *T*, it can be present at high concentration without influencing the effective signal transduction in the **Threshold Controller**. For instance, the concentration of *A* in the following regulation reactions was set at 800 nM, which is 20 times higher than that of *T*. Thus, the strategy of the amplification delay step is to maintain the correct reaction order between the **Threshold Controller** and the **Inhibition Generator**, while producing sufficient TA-15 to perform the inhibition function.

To demonstrate the function of the circuit with threshold control of blood coagulation in the presence of excessively high thrombin concentrations, two parallel threshold concentrations of 100 and 200 nM were tested. Below the threshold value, the system should perform the normal coagulation function as thrombin alone. Once the thrombin concentration exceeds the threshold value, inhibition is actuated with the release of TA-15, and the hydrolysis rate of the substrate is attenuated (monitored by absorbance at 405 nm, as shown in Figure S10). The absorbance changes (δA) after 30 min for different thrombin concentrations are summarized in Figure 6a. Without the aptamer circuit, larger δA values were found with higher thrombin concentrations. In the presence of the threshold
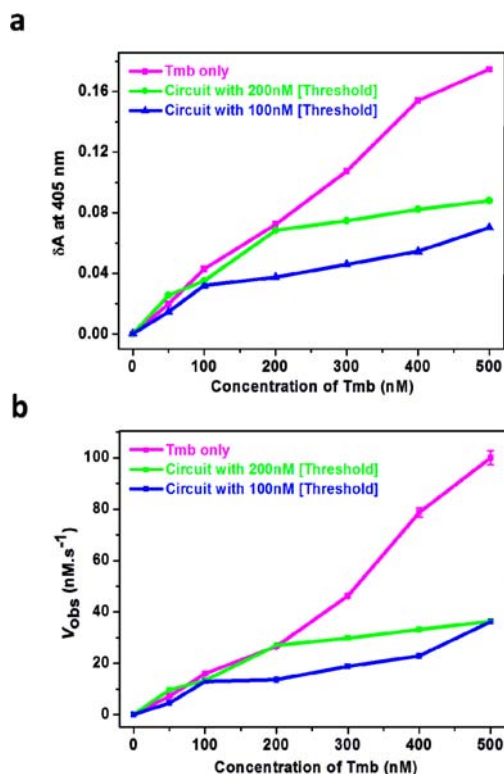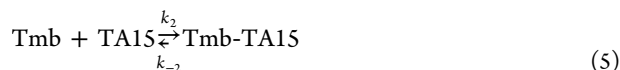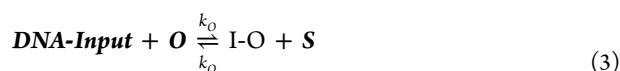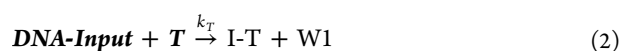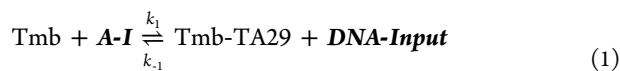

Figure 6. (a) Absorbance changes (δA) of chromogenic peptide substrate upon different thrombin concentrations with and without circuit. (b) V_{obs} of the enzymatic reaction upon different thrombin concentrations with and without circuit. Purified *A-I*, *O*, *A*, *G*, and *F* were mixed at concentrations of 100, 100, 800, 800, and 800 nM, respectively. *T* was set at either 20 or 35 nM for circuits with two different threshold values.

control circuit, but below the threshold concentration, δA kept increasing with increasing thrombin concentration, showing similar behavior to that of thrombin alone. However, once the threshold value has been exceeded, the activity of redundant thrombin was effectively inhibited, resulting in a nearly constant, or slightly increased, δA value compared to that of threshold thrombin. The sharp turning point can be observed exactly at our preset threshold value. Using the 200 nM threshold as an example (green line in Figure 6a), the green line is nearly identical to the purple line of thrombin alone below 200 nM thrombin input, indicating that the thrombin works freely at this stage. However, in the absence of the circuit, when the thrombin concentration was increased from 200 to 500 nM, the δA value was also increased by 141.1%. Otherwise, in the presence of the molecular circuit, it rose only slightly (28.6%), exhibiting a 5-fold difference in activity for the excess portion. A

similar trend was observed for a threshold of 100 nM, although the inhibition capability was slightly weaker at higher thrombin concentrations. This is probably caused by the greater total concentration of thrombin needed for inhibition with a lower threshold value, as well as the limited amount of inhibitor the circuit can generate. This problem could be circumvented by presetting with a higher concentration of the **Inhibitor Generator** module. In addition, we further investigated the initial reaction rates (V_{obs}) of this enzymatic reaction. The V_{obs} calculated from the slope of the initial linear portion of the absorbance kinetics also exhibited consistent results (Figure 6b). These data strongly demonstrated that effective inhibition starts when the threshold is exceeded and only acts on redundant enzymes, confirming the smart inhibitory function of this molecular circuit.

Theoretical Reaction Calculations. For rational engineering of an effective molecular circuit, it is important to derive kinetic reaction equations and competitive equilibrium expressions to better understand and predict system behavior. Therefore, we analyzed the reactions in our circuit, which are summarized below. The designed reactions include (1) a reversible binding reaction between thrombin and *A-I*; (2) an irreversible thresholding strand displacement reaction with fast k_T associated with 11-nt toehold; (3) a reversible outputting strand displacement reaction with slow forward and backward k_O associated with 5-nt toehold, which can be driven forward by a *Fuel* strand; (4) an irreversible inhibitor generation strand displacement reaction with forward k_G associated with 5-nt toehold; and, finally, (5) an inhibition reaction between TA15 and thrombin. Herein, reactions (1) and (5) are individual reactions which do not influence each other. The elementary steps may be written as:

$$\text{Tmb} + \textbf{\textit{A-I}} \underset{k_{-1}}{\overset{k_1}{\rightleftharpoons}} \text{Tmb-TA29} + \textbf{\textit{DNA-Input}} \tag{1}$$

$$\textbf{\textit{DNA-Input}} + \textbf{\textit{T}} \overset{k_T}{\rightarrow} \text{I-T} + \text{W1} \tag{2}$$

$$\textbf{\textit{DNA-Input}} + \textbf{\textit{O}} \underset{k_O}{\overset{k_O}{\rightleftharpoons}} \text{I-O} + \textbf{\textit{S}} \tag{3}$$

$$\textbf{\textit{S}} + \textbf{\textit{G}} \overset{k_G}{\rightarrow} \text{TA15} + \text{W2} \tag{4}$$

$$\text{Tmb} + \text{TA15} \underset{k_{-2}}{\overset{k_2}{\rightleftharpoons}} \text{Tmb-TA15} \tag{5}$$

On the basis of the theoretical calculations shown in the Supporting Information, as an independent reaction, reaction 1 can reach the equilibruim within 30 min (Figure S2A), which correlates with the practical experiment results (Figure S6), indicating that reaction 1 occurs relatively rapidly. Reaction 5 can reach equilibruim even more rapidly than reaction 1, with $t_{1/2}$ of 250 s based on our simple kinetic predictions (Figure S2B). For reactions 2, 3 and 4, as studied by Qian and Winfree,[5] $k_T = 2 \times 10^6$ M^{-1} s^{-1} with the toehold length of 11 nt; $k_O \approx k_G \approx 5 \times 10^4$ M^{-1} s^{-1} with the toehold length of 5 nt. The reaction kinetics can be simulated using the built-in numerical integration algorithms.[39,40] After the simulation, we found that reactions 2−4 achieve equilibruim in 4−5 h, which is much slower than reactions 1 and 5. Thus, reactions 2−4 based on DNA strand displacement are the rate-limiting steps of the system.

For practical applications of the circuit to control the coagulation function of thrombin, a rapid response to the thrombin concentration fluctuation is necessary. To improve system response, it is necessary to accelerate reactions 2−4. Optimized sequence design may be considered, such as increasing the toehold numbers of *O* and *G* in reaction 3 and 4, respectively. But this needs to be balanced with the sensitivity of threshold control. A better solution would be to assemble the circuit modules on a scaffold, where DNA species can intereact without diffusion, and the local concentration of DNA strands can be increased.

In addition, the relatively insensitive response of reaction 1 to thrombin decreased the effectiveness of the threshold control in the entire circuit. Further mathematical calculations were performed and revealed that the intrinsic limitation for *DNA-input* generation is the equilibruim constant K_{eq} of reaction 1 (Supporting Information). To address the important design question regarding obtaining sufficient *DNA-input* and promoting the high Δ[*DNA-input*] generation upon different concentrations of thrombin for effective threshold control, we can plot the Δ[*DNA-input*] triggered by high concentration of thrombin (with a = 4, for example, where a is the ratio of [Tmb] and [*A-I*]) and low concentration of thrombin (a = 0.5) with varying K_{eq} (Figure S3B,C). Closer examination of the Δ[*DNA-input*] with varying K_{eq} reveals a clearly defined local maximum ($K_{eq} \approx 6.7$) that establishes the Δ[*DNA-input*] values for which the difference between the high thrombin concentration and low thrombin concentration is optimal. To further lower the threshold control for thrombin concentration, a reaction with higher K_{eq} is desired, and this is related to the binding affinity of the aptamer to thrombin, as well as the dissociation of the *A-I* duplex. Therefore, a better aptamer with higher affinity to thrombin would lower the threshold control concentration in our circuit. Another possible solution is to reduce the base pair numbers in the *A-I* duplex for easier release of *DNA-input* upon target−aptamer binding. But the functional domain on *DNA-input* still needs to be effectively blocked in the *A-I* duplex to avoid undesired leaking reactions.

■ CONCLUSION

Design of smart protein manipulation methods with such capabilities as specific recognition of target proteins, precise and autonomous control of protein function, and effective suppression of hyperactive enzymatic effects is an important step toward personalized and intelligent disease treatment.[41] In this study, we have successfully designed a threshold-control molecular circuit and achieved autonomous, self-sustained, and programmable manipulation of the catalytic activity of thrombin. This is the first molecular logic circuit based on direct NA−protein interactions for the manipulation of protein activities. On the basis of the flexible modularity, each module can work relatively independently, while their coordinated operation drives the entire circuit properly. By simply replacing or adding new modules, other functions may be feasible.

Compared with circuits based totally on base-pairing,[15,42,43] the introduction of an aptamer provides a direct molecular bridge linking DNA with proteins and enzymatic reactions, enabling precise sensing of the local enzymatic environment and smart regulation in situ. Moreover, as a variety of aptamers are either available or can be obtained through SELEX to bind a broad range of targets with tunable binding ability, the aptamer circuit developed here can be used as a powerful tool for constructing ligand-controlled regulation systems tailored to

respond to specific targets in defined situations. Although, in its current state, the circuit works only in the test tube, it can be combined with advanced DNA nanotechnology for further in vivo experiments. For instance, all these modules can be molded onto a DNA scaffold, such as DNA origami,[44,45] to build a complete system and facilitate the coordinated operation. Given the tunable regulation, design modularity and target specificity, the prototype aptamer circuit demonstrated here has the potential to enhance DNA technology with new insights and will broaden the utility of DNA circuits for applications in biology, biotechnology, and biomedicine.[46]

■ EXPERIMENTAL SECTION

DNA Synthesis. The DNA sequences were synthesized on the ABI 3400 DNA synthesizer. The synthesis protocol was set up according to the requirements specified by the reagents' manufacturers. Following on-machine synthesis, the DNA products were deprotected and cleaved from CPG by incubating with 2.5 mL of concentrated ammonium hydroxide for 17 h at 40 °C in water bath. The cleaved DNA product was transferred into a 15 mL centrifuge tube and mixed with 250 μL of 3.0 M NaCl and 5.0 mL of ethanol, after which the sample was placed into a freezer at −20 °C for ethanol precipitation. Afterward, the DNA product was spun at 4000 rpm under 3 °C for 20 min. The supernatant was removed, and the precipitated DNA product was dissolved in 500 μL of 0.2 M trithylamine acetate (TEAA Glen Research Corp.) for HPLC purification. The HPLC purification was performed with a cleaned Alltech C18 column on a Varian Prostar HPLC machine. The collected DNA product was dried and processed for detritylation by dissolving and incubating in 200 μL of 80% acetic acid for 20 min. The detritylation DNA product was mixed with 400 μL of ethanol and dried by a vacuum dryer. The DNA products were quantified and stored in DNA water for subsequent experiments. The detailed sequences information is described in Supporting Information (Table S1 and S2).

DNA Purification. Native PAGE was applied to purify the Aptamer-Input, Threshold, Output and Generator duplex strands to remove excess strands and avoid undesired system leakage. The ssDNA components of **A-I**, **T**, **O**, and **G** were annealed at concentrations of around 50 μM in 1× TAE-Mg buffer (40 mM Tris-Acetate-EDTA, pH 8.0, 12.5 mM Mg(Ac)$_2$). Native PAGE gels (12%) in 1× TAE-Mg buffer were run at 110 V for 90 min at 4 °C and stained with GelRed stain solution (Biotium, CA). Only the sharp bands were cut from the gels, chopped into small pieces, and soaked in 1× TAE-Mg buffer for 24 h. After soaking out most DNA molecules from the gel pieces, the solutions were extracted and concentrated with centrifugal filter devices (Millipore, MA). Finally, the DNA duplex sequences were quantified by UV spectrometry and kept in buffer for future use.

Quantitative Analysis of Released *DNA-Input* Strands Triggered by Thrombin. A 100 μL sample of 100 nM **A-I** probes was placed in thrombin buffer containing 1× TAE with 100 mM NaCl, 12.5 mM MgCl$_2$, 10 mM KCl, and 1 mM CaCl$_2$. Different amounts of thrombin were incubated with the probes, and the fluorescence was monitored. To quantify the released *DNA-input*, 1 mL of 500 nM FAM-**TA-29** and 1 mL of 500 nM DABCYL-*DNA-input* were annealed in thrombin buffer to make the FRET **A-I** duplex solution. Then, **A-I** duplex was purified with gel electrophoresis. Different concentrations of thrombin (0−500 nM) and 100 nM purified **A-I** were mixed and diluted to 100 μL in thrombin buffer. Fluorescence was tested after incubation for 3 h by using Fluorolog (Jobin Yvon Horiba). In the experiment of making calibration curve, different concentrations of FAM-labeled **TA-29** (0−100 nM) were prepared in 100 μL of thrombin buffer solution, and the fluorescence was measured after 3 h.

Validation of Signal Transduction by Fluorescence. When the signal transduction process in the **Inhibitor Generator** module was tested, **O** (100 nM), **G** (150 nM), and **F** (200 nM) were mixed in 1× TAE-Mg buffer to the total volume of 100 μL, and the fluorescence

was monitored in the absence and presence of 100 nM **DNA-input**. The fluorescence intensities of the system with different concentrations of **DNA-input** under the same condition were also measured. When the signal transduction process in the **Threshold Controller** module was tested, 40 nM **T** was added to the solution described above, and fluorescence was monitored with the concentrations of **DNA-input** at 0, 40, 50, 60, 100, and 200 nM. When thrombin was used as input, the buffer was changed to thrombin buffer. Different concentrations of thrombin (0−500 nM) were first incubated with **A-I** for 1 h. Then, **O** (100 nM), **G** (150 nM), **F** (200 nM), and **T** (20 or 35 nM) and thrombin buffer were mixed to the total volume of 100 μL. Fluorescence intensities were tested after incubation for 3 h at room temperature.

Thrombin Catalytic Activity Assay. The hydrolysis experiment of β-Ala-Gly-Arg-*p*-nitroanilide diacetate (Sigma-Aldrich) was carried out in thrombin buffer. First, 1 μL of thrombin was taken from 10 μM stock solution, diluted to 196 μL, and incubated at room temperature for 10 min (50 nM). Then, 4 μL of 0.5 mM chromogenic peptide substrate β-Ala-Gly-Arg-*p*-nitroanilide diacetate) was mixed with the thrombin solution to make the final concentration of 10 μM. The hydrolysis rate of the substrate was determined by monitoring the absorbance at 405 nm using Cary 100 spectrometry (Varian) with a 200 μL macro cuvette. The rates for different thrombin concentrations were tested in the same way (Figure S7). When testing the inhibition effect of **TA-15** to thrombin, thrombin was incubated with different concentrations of **TA-15** and **TA-29** in buffer for 1 h. Then, chromogenic peptide substrate was added, and the absorbance was monitored at 405 nm (Figure S8). The hydrolysis rate of thrombin with the aptamer circuit was determined in the thrombin buffer containing 1× TAE with 100 mM NaCl, 12.5 mM MgCl$_2$, 10 mM KCl, and 1 mM CaCl$_2$. At the threshold of 100 nM (thrombin concentration), a 20 μL sample of 1 μM **A-I** was incubated with 2 μL of 10 μM thrombin in thrombin buffer for 3 h. Then, 20 μL of 8 μM **A**, **G**, and **F**, 20 μL of 200 nM **T**, and 20 μL of 1 μM **O** were added, and the total volume of solution was made to 196 μL with thrombin buffer. The mixture was incubated at room temperature for 6 h. At the threshold of 200 nM (thrombin concentration), the volume of **T** was changed to 35 μL, and all other conditions were kept constant. Then, 4 μL of 0.5 mM chromogenic peptide substrate (final concentration: 10 μM) was added, and the hydrolysis rate was determined by monitoring the absorbance of mixtures at 405 nm at room temperature. The rates for different thrombin concentrations were tested in a similar way (Figure S10).

■ ASSOCIATED CONTENT

Ⓢ Supporting Information
Theoretical reaction calculations, results of fluorescence characterization of the circuit and the time-dependent absorbance spectrum of thrombin catalytic activity. This material is available free of charge via the Internet at http://pubs.acs.org.

■ AUTHOR INFORMATION

Corresponding Author
tan@chem.ufl.edu

Author Contributions
§These authors contributed equally to the work.

Notes
The authors declare no competing financial interest.

■ ACKNOWLEDGMENTS

■ REFERENCES

(1) Isaacs, F. J.; Dwyer, D. J.; Collins, J. J. *Nat. Biotechnol.* **2006**, *24*, 545.

(2) Seelig, G.; Soloveichik, D.; Zhang, D. Y.; Winfree, E. *Science* **2006**, *314*, 1585.

(3) Zhang, D. Y.; Turberfield, A. J.; Yurke, B.; Winfree, E. *Science* **2007**, *318*, 1121.

(4) Zhang, D. Y.; Winfree, E. *Nucleic Acids Res.* **2010**, *38*, 4182.

(5) Qian, L.; Winfree, E. *Science* **2011**, *332*, 1196.

(6) Ran, T.; Kaplan, S.; Shapiro, E. *Nat. Nanotechnol.* **2009**, *4*, 642.

(7) Beisel, C. L.; Bayer, T. S.; Hoff, K. G.; Smolke, C. D. *Mol. Syst. Biol.* **2008**, *4*, 224.

(8) Kolpashchikov, D. M.; Stojanovic, M. N. *J. Am. Chem. Soc.* **2005**, *127*, 11348.

(9) Stojanovic, M. N.; Kolpashchikov, D. M. *J. Am. Chem. Soc.* **2004**, *126*, 9266.

(10) Benenson, Y.; Gil, B.; Ben-Dor, U.; Adar, R.; Shapiro, E. *Nature* **2004**, *429*, 423.

(11) Gil, B.; Kahan-Hanum, M.; Skirtenko, N.; Adar, R.; Shapiro, E. *Nano Lett* **2011**, *11*, 2989.

(12) Saghatelian, A.; Guckian, K. M.; Thayer, D. A.; Ghadiri, M. R. *J. Am. Chem. Soc.* **2003**, *125*, 344.

(13) Win, M. N.; Smolke, C. D. *Science* **2008**, *322*, 456.

(14) Carothers, J. M.; Goler, J. A.; Juminaga, D.; Keasling, J. D. *Science* **2011**, *334*, 1716.

(15) Xie, Z.; Wroblewska, L.; Prochazka, L.; Weiss, R.; Benenson, Y. *Science* **2011**, *333*, 1307.

(16) Stricker, J.; Cookson, S.; Bennett, M. R.; Mather, W. H.; Tsimring, L. S.; Hasty, J. *Nature* **2008**, *456*, 516.

(17) Freeman, M. *Nature* **2000**, *408*, 313.

(18) Culler, S. J.; Hoff, K. G.; Smolke, C. D. *Science* **2010**, *330*, 1251.

(19) Ellington, A. D.; Szostak, J. W. *Nature* **1990**, *346*, 818.

(20) Tuerk, C.; Gold, L. *Science* **1990**, *249*, 505.

(21) Robertson, D. L.; Joyce, G. F. *Nature* **1990**, *344*, 467.

(22) Vuyisich, M.; Beal, P. A. *Chem. Biol.* **2002**, *9*, 907.

(23) Lee, J. H.; Canny, M. D.; De Erkenez, A.; Krilleke, D.; Ng, Y. S.; Shima, D. T.; Pardi, A.; Jucker, F. *Proc. Natl. Acad. Sci. U.S.A.* **2005**, *102*, 18902.

(24) Green, L. S.; Jellinek, D.; Jenison, R.; Ostman, A.; Heldin, C. H.; Janjic, N. *Biochemistry* **1996**, *35*, 14413.

(25) Lee, J. F.; Stovall, G. M.; Ellington, A. D. *Curr. Opin. Chem. Biol.* **2006**, *10*, 282.

(26) Nie, X.; Castanares, M.; Mukherjee, A.; Lupold, S. *Curr. Med. Chem.* **2011**, *18*, 4206.

(27) Hirsh, J. *Thromb. Res.* **2003**, *109* (Suppl. 1), S1.

(28) Bock, L. C.; Griffin, L. C.; Latham, J. A.; Vermaas, E. H.; Toole, J. J. *Nature* **1992**, *355*, 564.

(29) Tasset, D. M.; Kubik, M. F.; Steiner, W. *J. Mol. Biol.* **1997**, *272*, 688.

(30) Zhang, D. Y.; Winfree, E. *J. Am. Chem. Soc.* **2009**, *131*, 17303.

(31) Zhang, D. Y.; Seelig, G. *Nat. Chem.* **2011**, *3*, 103.

(32) Nutiu, R.; Li, Y. *J. Am. Chem. Soc.* **2003**, *125*, 4771.

(33) Tang, Z.; Mallikaratchy, P.; Yang, R.; Kim, Y.; Zhu, Z.; Wang, H.; Tan, W. *J. Am. Chem. Soc.* **2008**, *130*, 11268.

(34) Wolberg, A. S. *Blood Rev.* **2007**, *21*, 131.

(35) Muller, J.; Becher, T.; Braunstein, J.; Berdel, P.; Gravius, S.; Rohrbach, F.; Oldenburg, J.; Mayer, G.; Potzsch, B. *Angew. Chem., Int. Ed.* **2011**, *50*, 6075.

(36) Ramjee, M. K. *Anal. Biochem.* **2000**, *277*, 11.

(37) Hsu, C. L.; Chang, H. T.; Chen, C. T.; Wei, S. C.; Shiang, Y. C.; Huang, C. C. *Chemistry* **2011**, *17*, 10994.

(38) Shiang, Y. C.; Hsu, C. L.; Huang, C. C.; Chang, H. T. *Angew. Chem., Int. Ed.* **2011**, *50*, 7660.

(39) Franco, E.; Friedrichs, E.; Kim, J.; Jungmann, R.; Murray, R.; Winfree, E.; Simmel, F. C. *Proc. Natl. Acad. Sci. U.S.A.* **2011**, *108*, E784.

(40) Seesaw Compiler Home page. http://www.dna.caltech.edu/SeesawCompiler/.

(41) Hood, L.; Heath, J. R.; Phelps, M. E.; Lin, B. *Science* **2004**, *306*, 640.

(42) Choi, H. M.; Chang, J. Y.; Trinh le, A.; Padilla, J. E.; Fraser, S. E.; Pierce, N. A. *Nat. Biotechnol.* **2010**, *28*, 1208.

(43) Dirks, R. M.; Pierce, N. A. *Proc. Natl. Acad. Sci. U.S.A.* **2004**, *101*, 15275.

(44) Rothemund, P. W. *Nature* **2006**, *440*, 297.

(45) Douglas, S. M.; Dietz, H.; Liedl, T.; Hogberg, B.; Graf, F.; Shih, W. M. *Nature* **2009**, *459*, 414.

(46) Venkataraman, S.; Dirks, R. M.; Ueda, C. T.; Pierce, N. A. *Proc. Natl. Acad. Sci. U.S.A.* **2010**, *107*, 16777.